AIChE

# Computational Study of Staged Membrane Reactor Configurations for Methane Steam Reforming. I. Optimization of Stage Lengths

**Alessio Caravella, Francesco Paolo Di Maio, and Alberto Di Renzo**
Dept. of Chemical and Materials Engineering, University of Calabria, Rende (CS) 87036, Italy

*DOI 10.1002/aic.11961*
*Published online November 9, 2009 in Wiley InterScience (www.interscience.wiley.com)*

*This article and Part II report a computational study carried out to analyze the performance achievable using a staged membrane reactor in the methane steam reforming process to produce high purity hydrogen. A reaction/separation unit in which reactive stages are laid out in series to permeative stages already proposed in literature (Caravella et al., J Memb Sci. 2008;321:209–221) is modified here to increase its flexibility. The improvement includes the consideration of the Pd-based membrane along the entire length. Two- and ten-staged reactors are examined in terms of methane conversion, hydrogen recovery factor and hydrogen recovery yield, considering co- and counter-current flow configurations. Individual stage lengths are obtained by maximizing either methane conversion or hydrogen recovery yield, comparing the results to the ones of an equivalent traditional reactor and a conventional membrane reactor. The analysis allows demonstrating that the counter-current configuration leads to significant improvements in the hydrogen recovery, but proves almost irrelevant with respect to methane conversion. The influence of the number of stages and the amount of catalyst is quantified in the accompanying part II article.* © 2009 American Institute of Chemical Engineers *AIChE J,* 56: 248–258, 2010

*Keywords: staged membrane reactor, catalyst distribution, steam reforming, hydrogen production*

## Introduction

The advantage of membrane reactors with respect to conventional units consists in their ability to combine two operations (i.e. reaction and selective separation) in one process unit and exploit, whenever possible, the simultaneous permeation to increase the conversion of reactants and the continuous generation of products to improve the separation efficiency.[1] This can lead to the possibility of achieving at the same time very high purification yields and conversions higher than the limiting equilibrium values typically encountered in traditional reactors, which could be substituted with innovative equipments being more compact and modular according with the process intensification strategy.[2] Advantages are particularly significant when highly selective membranes are available for the purpose. This is the case of the high purity hydrogen production by hydrocarbon steam reforming, as the palladium-based membranes are capable of performing hydrogen separation with the desired purity. In the forthcoming hydrogen era, mainly pushed towards zero-emission combustion engines and high efficiency fuel cells, the use of membrane reactors to carry out reforming of methane appears an extremely promising technology. Several research groups have contributed to the study and characterization of such membranes with the aim to maximize their performance and solve technological problems related to their preparation,[3,4] surface stability[5,6] and inhibition or poisoning effect.[7–9] In this sense, many researchers are

Correspondence concerning this article should be addressed to A. Caravella at alessio.caravella@unical.it

interested in the integration of appropriate membranes in processes involving hydrocarbons steam reforming, and different models have been used to simulate the so-assembled membrane reactors. The effect of several operating conditions (total pressure, membrane characteristics, sweep ratio) have been already investigated by means of more or less complex models in order to establish the conditions to maximize the performance of this type of equipments. In particular, Koukou et al.[10] analyzed the role of nonideal flow in membrane reactors, showing the importance of taking into account the radial profiles when a high radial dimension is considered. A similar study was carried out by Assabumrungrat et al.[11] in their article on the oxidative dehydrogenation of *n*-butane in a porous membrane reactor, where the effect of several other factors like furnace temperature, air/*n*-butane feed ratio and reactor size is analyzed. Some of other simulation studies were carried out in parallel with experimental analyses. Among the simulation works, the influence of the heat transfer due to the $H_2$ permeating flux through Pd-alloy membranes was considered by Marigliano et al.,[12] whereas Lin et al.[13] studied the effect of incipient removal of hydrogen. Oklany et al.[14] considered two different membranes (a Pd-based membrane and a microporous one), whilst Adris et al.[15] carried out the methane steam reforming in a fluidized-bed membrane reactor at high temperature. Chiappetta et al.[16] analyzed the importance of the catalyst axial distribution on the temperature hot spot along a packed bed Pd-membrane reactor performing the Water gas shift. In their article, they considered three different axial distributions: constant, linear and exponential, finding that it is more useful to adopt a linear catalyst distribution in order to control the hot spot. However, only recently the potential of the operation under staged conditions has been recognized as a possibility to increase the overall reactor performance. For hydrogen production by methane steam reforming, Caravella et al.[17] showed that, the use of reaction and permeation zones in series, can — in some case significantly — enhance the final result. This results from two aspects that can be simplified as follows: on one hand, the presence of intermediate permeative zones contributes to shift the conditions far from equilibrium in the subsequent reaction stages, thereby re-enabling fast kinetics; on the other hand, the intermediate conversion of reactants towards the permeable products allows a larger driving force to be established in the permeative stages, leading to an increased separation yield. The cumulative effect of such a combination can be appreciable in terms of overall conversion and hydrogen recovery yield (RY), especially when optimized stage lengths are used.[17] However, the use of a staged membrane reactor introduces a number of issues that need to be addressed. First of all, the technological problems are related to the assembly of permeative and nonpermeative stages along the same tubular unit. This issue is particularly relevant when considered in combination to the low flexibility of the optimal distribution of the stage lengths. A change in the operating conditions would in fact need the used of a reoptimized length distribution or, in other words, a new reactor. Another application of the concept of staged membrane reactor was proposed by Li et al.,[18] although in their scheme the four stages are connected in such a way that the reactive stages are placed within a furnace and the permeative ones within another furnace. However, such an arrangement would in any case require two distinct process units. As an attestation of the continuously increasing importance of the staged membrane reactors, several national and international patents have been already developed or are still under development.[19–21] This fact highlights the technological improvements able to be led up by analyzing innovative staged equipments. In this direction, the objective of the present work is to analyze a tubular staged reactor in which the membrane crosses the entire reactor and a series of stages is considered only in the feed side of the reactor. Differently from the article of Caravella et al.,[17] who focussed on the effect of temperature and membrane thickness, the effect of the flow configuration (co- or counter-current) will also be investigated. By making use of a similar model, the optimization procedure will be applied here to determine the stage length distribution that maximizes the conversion and the one maximizing the hydrogen RY. Other important aspects, including the overall amount of catalyst and the number of stages, will be investigated in the accompanying part II of this work.[22]

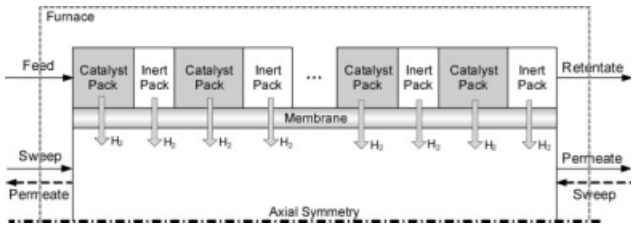


**Figure 1. Scheme of the staged membrane reactor (SMR) considered.**

### *Description of the system*

Starting from the idea of a staged membrane reactor to carry out the steam reforming of methane (Caravella et al.[17]), a new reactor configuration is proposed here. In fact, the original series of distinct reactive-only and permeative-only stages poses considerable problems when it comes to the physical realization of the reactor assembly, primarily regarding the connections between the tubular permeable and nonpermeable elements (typically of different materials). It is therefore interesting to examine the performance of a reactor in which the membrane represents the whole tube (like in conventional membrane reactors) and the shell side is composed of a series of reactive and inert stages (Figure 1). In this way the reactor geometry is much simpler and the complexity is left only to the realization of the catalyst and inert stages. However, this can be rather easily realized, for example, by vertical deposition of successive reactive and inert particle layers with the appropriate proportions.

With respect to the distinct-stage reactor (i.e. the PSMR[17]), the proposed unit will be a sequence of reactive-permeative stages and permeative-only ones. As a consequence, it will be not possible to compare it to the conventional membrane reactor under equivalent conditions (i.e. with the same amount of catalyst and membrane area). As will be discussed in the "Results and discussions" section, the comparison against conventional units will be carried out by considering the same membrane length, i.e. the same

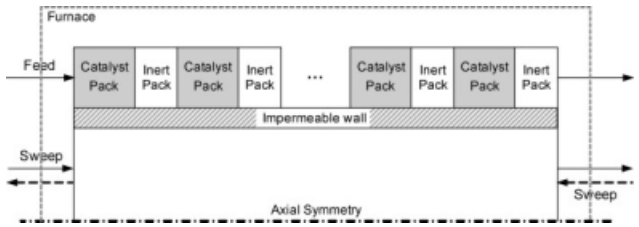


**Figure 2. Scheme of a staged traditional reactor with a structure similar to the SMR shown in Figure 1.**

reactor length. The presence of inert stages results in a catalyst amount that will be lower than the corresponding membrane reactor. A two- and a ten-stage reactor will be analyzed in details, both containing a total of the 50% of the overall (shell) volume. Most of the analysis on the optimal reactive stage length distributions will be carried out by focussing on the effect of the optimization variable chosen and on the influence of the flow configuration, considering a corresponding tubular impermeable staged reactor as a reference (see Figure 2). The assessment of the loss of performance of the staged reactor vs. the fully filled membrane reactor will be discussed later, but a more detailed comparison under more favourable conditions can be found in part II of this work.[22]

For the rest of the system, a reference experimental work will be considered as a data source.[23] The reactor is located inside a furnace where the temperature is assumed to be controlled at a set value. The reaction mechanism of the methane steam reforming on Ni-based catalyst is taken from the work of Xu and Froment[24]:

$$\begin{aligned} &CH_4 + H_2O \Leftrightarrow CO + 3H_2 && \Delta H_r^0 = 206 \text{ kJ/mol} \\ &CO + H_2O \Leftrightarrow CO_2 + H_2 && \Delta H_r^0 = -41.4 \text{ kJ/mol} \\ &CH_4 + 2H_2O \Leftrightarrow CO_2 + 4H_2 && \Delta H_r^0 = 165 \text{ kJ/mol} \end{aligned} \quad (1)$$

The here-considered membrane, present in both reactive and inert zones, is a supported Pd-based membrane, whose permeation characteristics are taken from the experimental work of Tong et al.[23] The mathematical representation of the system is discussed in the next section.

### *Mathematical model*

The model used in the present study represents an extension of the one already described in detail and validated elsewhere.[17] It consists in a one-dimensional nonisothermal model including multicomponent mass balances, energy and momentum balance along the reactor, assuming the plug-flow conditions. Methane steam reforming is a very fast reaction and this leads to abrupt concentration changes, typically accounted for by means of an axial dispersion model. However, under the operating conditions of the examined cases, the convection contribution dominates the axial transport as the longitudinal Peclet number ($v \times L^{Tot}/D$) exceeds 1000.[25] The heat transfer is considered among all the reactor sections and from/to the furnace, with temperature-dependent physical properties and permeance. The main enhancement over the previous model[17] is related to the possibility of solving for the counter-current configuration. Furthermore, a more general correlation, also accounting for the particle-to-shell diameter ratio, is used for heat transfer calculation (see Appendix A). The key model features will be shortly summarized in the following subsections.

### *Set of equations*

The equations relative to the mass balances for both reactive and inert stages are:

$$\begin{aligned} \frac{dF_i^{Ret}}{dz} &= R_i A^{Ret} - N_i^{Mem} \pi D_m^{Mem} \\ \frac{dF_i^{Perm}}{dz} &= N_i^{Mem} \pi D_m^{Mem} \end{aligned} \quad (2)$$

with

$$N_i^{Mem} = \begin{cases} 0, & i \neq H_2 \\ N_{H_2}, & i = H_2 \end{cases} \quad (3)$$

and the reaction rate of the $i$th species, $R_i$, is set to zero in the inert stages. The quantities $F_i^{Ret}$ and $F_i^{Perm}$ are the axial molar flow rate of the ith species in the retentate and permeate, respectively, and $N_{H_2}$ is the $H_2$ permeating flux through the Pd-alloy membrane. The permeation law used is[23]:

$$N_{H_2} = \frac{\kappa}{\delta^{Mem}} \exp\left(-\frac{E_d}{RT^{Mem}}\right)\left[\left(P_{H_2}^{Ret}\right)^{\alpha} - \left(P_{H_2}^{Perm}\right)^{\alpha}\right] \quad (4)$$

where $T^{Mem}$ is the membrane temperature, calculated as arithmetic mean of retentate and permeate temperature. The other parameters have the following values: $\kappa = 240 \times 10^{-10}$ mol m$^{-1}$ s$^{-1}$ Pa$^{-1}$, $E_d = 17563$ J mol$^{-1}$, and $\alpha = 1$. It can be noticed that Eq. 4 describes a permeating flux that does not obey the widely accepted Sieverts' law and the reasons for that can be various, as reported elsewhere (e.g.[26,27]). The energy balances for the retentate and the permeate side are:

$$\begin{aligned} \frac{d}{dz}\left(\sum_{i=1}^{m^{Ret}} F_i^{Ret} \Delta H_i^{Ret}\right) &= U^{Ext} \pi OD^{Shell}\left(T^{Furnace} - T^{Ret}\right) \\ &- U^{Mem} \pi OD^{Tube}\left(T^{Ret} - T^{Perm}\right) + -\pi D_m^{Mem} N_{H_2}^{Mem} \Delta H_{H_2}\big|_{T^{Ret}} \end{aligned} \quad (5)$$

$$\begin{aligned} \frac{d}{dz}\left(\sum_{i=1}^{m^{Perm}} F_i^{Perm} \Delta H_i^{Perm}\right) &= U^{Mem} OD^{Mem} \pi\left(T^{Ret} - T^{Perm}\right) \\ &+ \pi D_m^{Mem} N_{H_2}^{Mem} \Delta H_{H_2}\big|_{T^{Ret}} \end{aligned} \quad (6)$$

Their form is the same for the reactive and inert stages, since the heat lost because of reaction is included in the enthalpy variation. The pressure drops along the reactor are evaluated by means of the expressions provided by Sodrè and Parise.[28] In the permeation side (where there is no catalyst or inert pellets) the pressure is considered as constant. The co-current case leads to an initial value problem, which has been solved by means of the Matlab® function "*ode15s*" able to deal with stiff systems like the present one.[29] Differently, the counter-current configuration leads to a boundary value problem (BVP), which has been solved by means of the Matlab® function "*bvp4c*", based on a fourth order

**Table 1. Definition of the Performance Indices**

| Factor | Description | Formal Definition | Mathematical Definition |
|---|---|---|---|
| $x$ | $CH_4$ conversion | $\frac{CH_4\,Converted}{CH_4\,Fed}$ | $1-\frac{F^{Ret}_{CH_4}}{F^{0}_{CH_4}}$ |
| RF | $H_2$ recovery factor | $\frac{H_2\,Recovered\,in\,the\,Permeate\,Side}{H_2\,Produced}$ | $\frac{F^{Perm}_{H_2}}{F^{Ret}_{H_2}+F^{Perm}_{H_2}}$ |
| RY | $H_2$ recovery yield | $\frac{H_2\,Recovered\,in\,the\,Permeate\,Side}{Maximum\,H_2\,Produced\,at\,total\,CH_4\,Conversion}$ | $\frac{F^{Perm}_{H_2}}{4F^{0}_{CH_4}}$ |

collocation method.[29] Both methods use a variable integration step algorithm to reach the desired tolerance. In the most complex cases examined, the number of discretization points can exceed 10,000.

### *Optimization procedure*

The model equations can be utilized to evaluate the reactor performance as a function of several variables. By choosing an objective function and defining the design variables, an optimal set of values can be determined using standard techniques. In the present work, a performance index will be selected as objective function and the stage length distribution (i.e. the individual stage lengths) as design variables, subjected to some physical constraints.

The assessment of the performances of a multifunctional operation such as a (staged) membrane reactor can be quite complex. There are various aspects that can be considered important, such as reactant conversion and permeation efficiency, and different priority can be attributed depending upon the other equipment involved in the process. Three different dimensionless indexes, i.e. methane conversion ($x$), hydrogen recovery factor (RF) and hydrogen RY, whose definitions are reported in Table 1, will be considered in the present analysis as performance assessment. The quantities $F^0_{CH_4}$ and $F_{CH_4}$ are the methane flow rate in the feed and retentate, whereas $F^{Ret}_{H2}$ and $F^{Perm}_{H2}$ are the $H_2$ molar flow rate in the retentate and permeate side, respectively.

For the two objective functions considered, the optimization problem is mathematically represented by:

$$\max_{l} x \quad \text{or} \quad \max_{l} \mathrm{RY} \tag{7}$$

s.t.:

$$\sum_{i=1}^{n^R} l_i^R = \frac{l^{Tot}}{2}, \quad \sum_{i=1}^{n^I} l_i^I = \frac{l^{Tot}}{2} \tag{8}$$

$$l^{Min} < l_i < \frac{l^{Tot}}{2} \tag{9}$$

where $l = \{l_1^R,\ldots,l_{n^R}^R,l_1^I,\ldots,l_{n^I}^R\}$, $l_i^R$ and $l_i^I$ are the lengths of the $i$th Reactive ($R$) and Inert ($I$) stage, respectively, $l^{Min}$ is the minimum length that a stage can reach and $l^{Tot}$ is the total reactor length. Notice that the total length of the catalyst bed is one-half the total reactor length, which, in turn, is equal to the membrane one. The presence of a minimum length arises from the necessity for each stage to have a nonzero integration domain. The optimization problem was solved in Matlab® by means of the "fmincon" function.[29] Since the problem is highly nonlinear and, hence, may exhibit multiple local extrema, several different initial guess vectors were used to find the global solution.

## Results and Discussions

The stage length distributions will be obtained for the different objective functions, starting from a two-stage case in which the catalyst is located entirely in the first half of the reactor. This will serve as a reference for the subsequent distributions. The operating conditions and the geometrical data of the equipments analyzed are summarized in Tables 2 and 3. The values of the $H_2O/CH_4$ feed ratio (=3), the working temperature and total pressure are chosen in order to be similar to the ones in the experimental works of Tong et al.[3,23]

### *Case 1: the catalyst mass entirely placed at the reactor inlet*

The first distribution analyzed has the whole amount of catalyst concentrated at the reactor inlet. This configuration will be set as reference in the comparison carried out in the subsequent sections.

In Figure 3 the hydrogen partial pressure profiles are shown in co- and counter-current flow on both reactor sides. Up to the end of the catalyst bed — i.e., up to an abscissa of 0.5 — hydrogen is produced and selectively removed through the membrane at the same time. When the reaction is sufficiently rapid (i.e., at the reactor inlet), the permeation process has no significant influence on the hydrogen profiles in the retentate and very high partial pressure gradients are found. As the reaction rate decreases and the amount of produced hydrogen increases, the permeation rate becomes comparable to the reaction one and, hence, the slope of the hydrogen profile in the reaction side decreases. In the inert zones only permeation occurs, causing the hydrogen

**Table 2. Operating Conditions**

| | Pressure (kPa) | | | | | | |
|---|---|---|---|---|---|---|---|
| Side | $H_2$ | $CH_4$ | $CO_2$ | $H_2O$ | CO | Total | Total Flow Rate (mmol/s) |
| Feed | – | 125 | – | 375 | – | 500 | 8 |
| Sweep | – | – | – | 120 | – | 120 | 8 |

$T^{Furnace} = 600°C$, $\varepsilon_{Bed} = 0.40$.

**Table 3. Geometrical Data of the System**

| $ID^{Tube}$ (mm) | $\delta^{Mem}$ ($\mu$m) | $\delta^{Supp}$ (mm) | $ID^{Shell}$ (mm) | $OD^{Shell}$ (mm) | $L^{Tot}$ (cm) | $d_p$ ($\mu$m) |
|---|---|---|---|---|---|---|
| 10 | 6 | 1.2 | 30 | 32 | 100 | 400 |

pressures to decrease in the retentate and increase on the other side.

In the co-current case, the hydrogen profile in the reactive zone is flatter than the one in counter-current, whilst, in the inert zone, its decrease in the second flow configuration is much higher than in the first one, allowing an almost complete hydrogen recovery in the counter-current case (Figure 3b). These important differences, that significantly influence the reactor performances, can be analyzed in more details by referring to Figure 4, where the hydrogen permeation driving force (DF) and transmembrane flux profiles are shown. The peculiarity of the counter-current configuration is to have a reactor zone where a negative DF is found (back-permeation from the permeate to the reaction side). This occurs since the hydrogen fed at the inlet is zero, whereas it is accumulated progressively in the permeate. Hence, a condition is created in which the DF is higher in those reactor zones where the reaction rate is slow, determining a better membrane exploitation. On the contrary, in co-current the DF is higher at the beginning of the reactor, where the kinetics is still fast and the presence of the membrane has less influence on the process. However, in terms of methane conversion, the advantage of the counter-current configuration disappears, as shown in Figure 5, where the two profiles reported can be hardly distinguished.

The analysis of the other performance indexes considered in this article allows the differences between the co- and counter-current flow to be appreciated (Figure 6). Along with the performance of the staged membrane reactors, also the one of the equivalent staged traditional reactor (TR) described in Figure 2 is reported for comparison in terms of conversion, since no indexes related to a hydrogen recovery degree can be defined for this equipment. It is useful to recall here that, when comparing the staged TR performances in the course of the article, we refer to a TR having the same distribution as the corresponding SMR considered in all of the subsequent sections. Observing Figure 6, although the conversion does not depend on the flow configuration (nor does it for the staged TR), this does influence the RY and, more strongly, the RF. In particular, from the co- to counter-current flow, RY increases by 9% ca., whilst the improvement in terms of RF is about 12%, reaching an almost complete hydrogen recovery. As concerns the comparison with the equivalent stage TR the advantage is doubtless. In the figure, both the flow configurations for the TR are reported, since their conversion values can be affected by the different temperature profiles.

In fact, in the case where the reaction and the permeation rate are comparable, the SMR allows an important increase of conversion and selective hydrogen recovery, which can be achieved even when the reaction is much faster than permeation. Furthermore, the very high value of RF (virtually the maximum achievable) could demonstrate that the distribution considered in this section is the one corresponding to the maximum RF. This is in analogy to what was found in a previous investigation,[17] where the maximization procedure of RF applied to a co-current permeative-stage membrane reactor provided a distribution with almost the whole catalyst mass concentrated at the beginning of the reactor.

### *Case 2: maximization of methane conversion*

Once the SMR has been analyzed in the reference distribution, an optimization procedure has been carried out by setting the methane conversion as objective function. Carrying out the optimization procedure described above, the distributions shown in Table 4 (in terms of stage lengths) are obtained. The corresponding profiles are shown in Figure 7

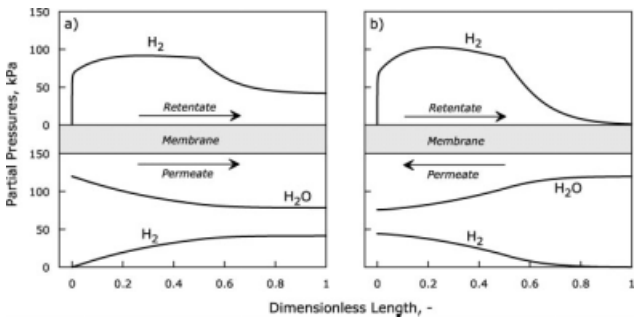


**Figure 3. $H_2$ and $H_2O$ (permeate only) partial pressure profiles along the reactor length in the reference configuration in (a) co- and (b) counter-current flow. The arrows indicate the sense of the stream flow.**

The operating conditions are specified in Table 2.

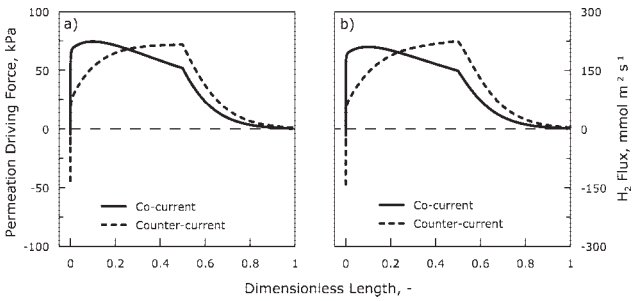


**Figure 4. (a) Hydrogen permeation driving force and (b) transmembrane flux profiles (positive from reaction to permeation side) along the reactor length in the reference configuration in co- and counter-current flow.**

The operating conditions are specified in Table 2.

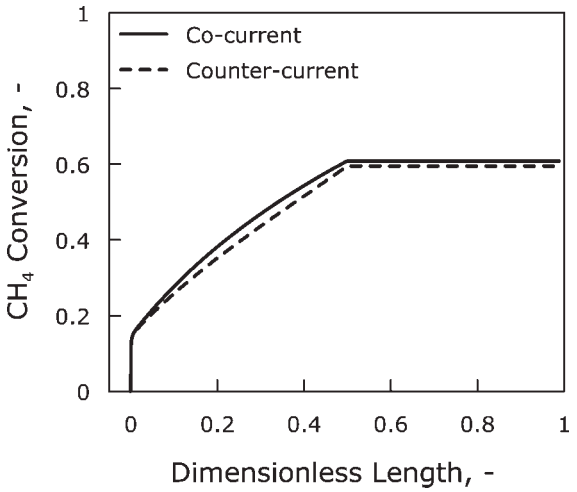


**Figure 5. Conversion profiles along the reactor length in the reference configuration in co- and counter-current flow.**

The operating conditions are specified in Table 2.

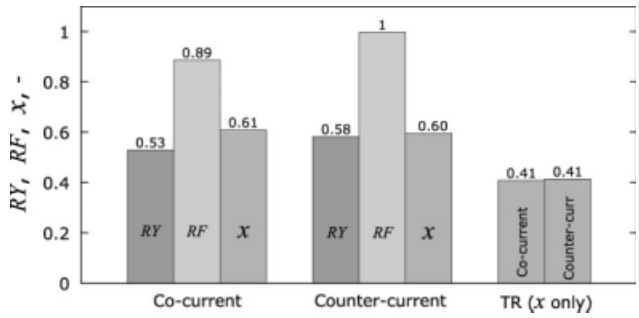


**Figure 6. Reactor performances in terms of recovery yield RY, recovery factor RF and conversion x in co- and counter-current flow in the reference catalyst distribution.**

The conversion of the corresponding staged TR is also reported for comparison in both the flow configurations. The operating conditions are specified in Table 2.

(in terms of partial pressure profiles) and in Figure 8 (in terms of conversion profiles). In this case, the situation is quite different than in the previous one. In fact, in co-current flow, a distribution with a very large first reactive stage is achieved, whilst, at the same time, the one in counter-current presents the largest reactive stage at the outlet.

As regards the reason of this opposite behavior, a possible explanation can be provided by looking at the temperature profiles (Figure 9). Generally speaking, it is reasonable to think that the procedure attempts to locate the largest catalyst packs in those zones where it is easier to acquire the energy required by the reaction, i.e., where the reaction temperature is the lowest. In the co-current flow this occurs towards the beginning of the reactor, where the sweep stream enters the reactor at the highest temperature. On the contrary, in counter-current flow this occurs towards the end, and, hence, the system exploits these favourable conditions as much as possible by allocating a large catalyst pack.

The other thing to notice is that, in both the cases, a negligible last inert stage is found. This fact, with the conversion as objective function, is somehow expected, since the inert stages do not provide any contribution to increase the conversion. Unfortunately, clear rules to predict the shape of an optimal distribution could not be identified, due to the complexity of the coupled phenomena involved in the process.

Analyzing the values of the performance indexes (Figure 10), a quite different situation with respect to the reference cases is found. The first thing to remark is that the conversions in co- and counter current are more different between each other (0.76 vs. 0.79) than the RFs (0.86 vs. 0.87). On the contrary, the difference of RY is still significant (about +10% for the counter-current flow). The conversions of the staged TRs are always independent of the flow configuration. With respect to the reference distribution, a lower value for the staged TR is found (0.45 vs. 0.41). This is due to the fact that, as mentioned above, in the inert stages the stream increases its temperature, creating more favourable conditions for the subsequent reactive stages. The higher is the number of stages, the more significant is this effect. As regards the TR in reference distribution (only two stages), there is no possibility for the reacting stream to exploit the amount of energy transferred in the inert stage, since, obviously, there are no other reactive stages after it. Of course, this is a trivial case, because there are no apparent reasons to build a TR with a useless pure heating stage, but it can be useful to understand the role of the distribution in a staged reactor. In other words, it can be said that the criterion by means of which the optimization procedure acts is an energetic criterion. At this regard, generally speaking, one can consider that the optimization procedure only redistributes the stages in such a way for the reactor to acquire the necessary heat (for reaction and/or permeation) in the most efficiently manner in dependence on the specific objective function chosen.

### *Case 3: maximization of the hydrogen RY*

The other objective function we chose to consider is the hydrogen RY. The shape of the optimal distribution is reported in Table 5 in terms of individual stage lengths list,

**Table 4. Optimal Lengths Distribution for the Maximum Conversion Criterion in Co- and Counter-Current Flow**

| | Stage Lengths, % of the Total Reactor Length | | | | | | | | | |
|---|---|---|---|---|---|---|---|---|---|---|
| Flow Configuration | $R_1$ | $I_1$ | $R_2$ | $I_2$ | $R_3$ | $I_3$ | $R_4$ | $I_4$ | $R_5$ | $I_5$ |
| Co-current | 22.7 | 13.6 | 1.2 | 14.3 | 12.8 | 11.4 | 3.2 | 10.7 | 10.1 | ≈0 |
| Counter-current | 1.6 | 6.8 | 6.5 | 14.5 | 6.5 | 12.6 | 1.9 | 16.1 | 33.5 | ≈0 |

The letters "*R*" and "*I*" indicate reactive and inert stages, respectively.

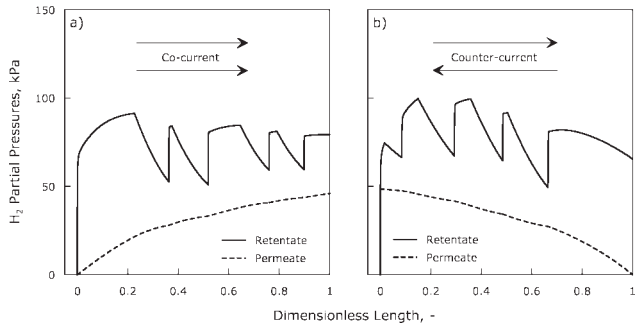


**Figure 7. $H_2$ and $H_2O$ partial pressure profiles along the reactor length for the distribution obtained from the maximization of the $CH_4$ in (a) co-current and (b) counter-current flow. The arrows indicate the sense of the stream flow.**

The operating conditions are specified in Table 2.

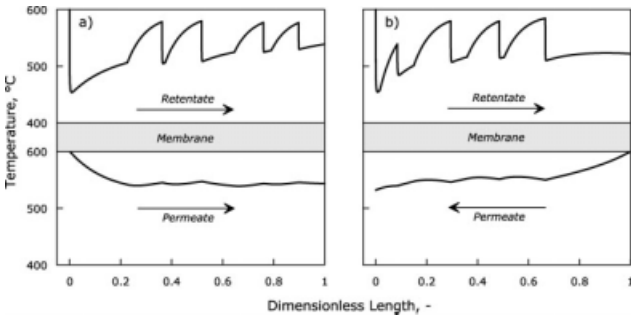


**Figure 9. Temperature profiles along the reactor length for the catalyst distribution obtained from the maximization of the $CH_4$ conversion in (a) co- and (b) counter-current flow.**

The arrows indicate the sense of the stream flow. The operating conditions are specified in Table 2.

where it can be observed that the optimal values can be considered, in a first approximation, as uniformly distributed. A possible explanation for this result is that maximizing the RY is, by its definition, equivalent to maximize the hydrogen content in the permeate and, thus, the permeating flux.

Therefore, the presence of too large reactive stages would imply the presence of other very short stages, which, especially towards the reactor outlet, would not allow a large amount of hydrogen produced and, hence, separated through the membrane. In this sense, it is not casual that, in both the flow configurations, the last reactive stage is little larger than all the previous ones. The resulting hydrogen profiles, corresponding to the optimal distributions, are shown in Figure 11. In each reactive zone, the reaction rate is very fast at the beginning and becomes slow towards the end. Considerations similar to the ones made earlier concerning the hydrogen content in the retentate are valid. In fact, also in this case the hydrogen partial pressure at the end of the SMR in counter-current flow is higher than in the co-current, and, for the same reasons, the profiles in counter-current are steeper. This becomes clear by examining the DF and permeating flux profiles (Figure 12). The plot in Figure 12 shows that, in the first part of the reactor, the DF in co-current is larger than the one in counter-current, but this tendency changes from a certain point on. In particular, in the reactive packs the DF profiles in co-current decrease, whilst those in counter-current increase significantly, causing a progressively larger gap. However, this important difference does not affect significantly the performance of the reactor in terms of conversion.

In fact, although the conversion profiles are quite different (Figure 13), the final values are practically the same. Hence, also in this case the conversion is not influenced by the configuration flow. Moreover, there is one more aspect to consider, namely the effect of the energy transfer. In fact, the role of the inert stages is to «recharge» the stream once it

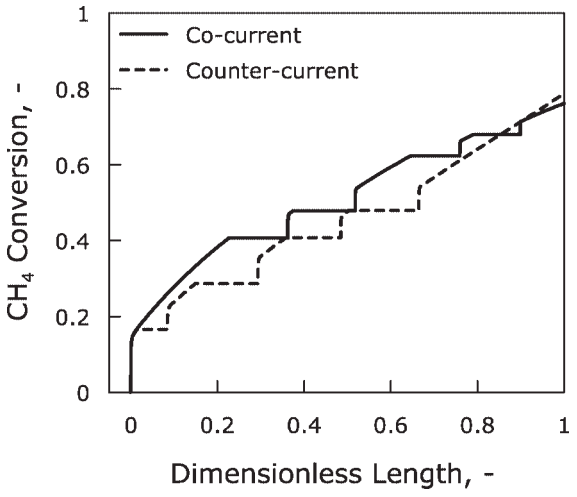


**Figure 8. Conversion profiles along the reactor length for the catalyst distribution obtained from the maximization of the $CH_4$ Conversion in co- and counter-current.**

The operating conditions are specified in Table 2.

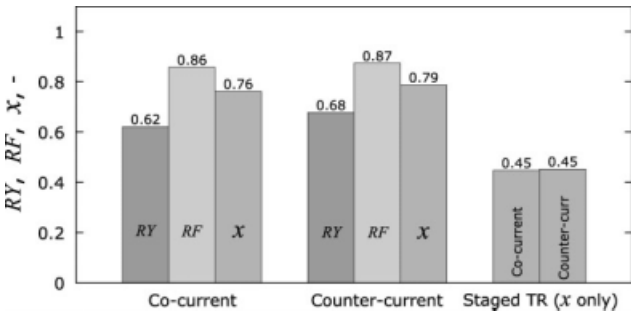


**Figure 10. Reactor performances in terms of recovery yield RY, recovery factor RF and conversion x in co- and counter-current flow for the catalyst distribution obtained from the maximization of *x*.**

The conversion of the corresponding staged TR is also reported for comparison in both the flow configurations. The operating conditions are specified in Table 2.

**Table 5. Optimal Lengths Distribution for the Maximum Recovery Yield Criterion in Co- and Counter-Current Flow**

| | Stage Lengths, % of the Total Reactor Length | | | | | | | | | |
|---|---|---|---|---|---|---|---|---|---|---|
| Flow Configuration | $R_1$ | $I_1$ | $R_2$ | $I_2$ | $R_3$ | $I_3$ | $R_4$ | $I_4$ | $R_5$ | $I_5$ |
| Co-current | 9.6 | 9.6 | 9.5 | 9.8 | 10.5 | 9.3 | 8.0 | 9.6 | 12.4 | 11.7 |
| Counter-current | 10.6 | 7.9 | 9.5 | 9.9 | 10.2 | 10.1 | 6.4 | 10.1 | 13.3 | 11.9 |

The letters "$R$" and "$I$" indicate reactive and inert stages, respectively.

has cooled down because of the reaction as well as allow a higher permeation through the membrane.

This last consideration arises from the fact that the permeating flux in an inert stage surely occurs at higher temperatures than the previous reactive stage. Thus, in these conditions, a lower permeation driving force is compensated by a higher permeance. The question about the energy transfer is of crucial importance also for the reactive stages, which require heat from the furnace and, in this specific case, from the permeate side. The overall effect of all these coupled kinetic and transfer phenomena affects the performance indexes as shown in Figure 14. One can notice the significant difference in terms of RY and RF between co- and counter-current. As regards RY, the counter-current flow provides an increase of 11% ca. with respect to the co-current case, while the improvement of RF is about 10%. These large gaps are determined by the different behavior of the system in terms of driving force and permeating flux analyzed above (Figure 12). The larger the permeation rate, the higher all the performance indexes related to the hydrogen recovery. As concerns the comparison with the corresponding TRs, the improvement is evident, showing a conversion increased by a factor of 0.30.

### *Comparison among the different distributions*

Once three different catalyst distributions have been analyzed, it is interesting to compare their performances in order to highlight the positive and negative aspects of each distribution. For the co-current flow, Figure 15 reports the three performance indexes considered in this article together with those of a conventional membrane reactor (MR), with the same membrane area as the SMR, but completely filled with catalyst. Obviously, the larger amount of catalyst causes the MR to overcome the performances of all the SMRs in terms of $x$ and RY. As concerns RF, the reference distribution is still the best, even considering the MR, whilst it is the worst one in terms of RY and $x$. This is due to the peculiarity of the two-stage reactor, which favours the permeative factor at the expense of the reactive one, since the energy is not transferred as much to increase the reaction rate but rather to get advantage to the permeation rate. However, an RF higher than the MR is not a surprising result, since, by its definition, it compares the hydrogen recovered in the permeate to the hydrogen produced by the reaction. Both of these quantities are variable and, in this case, the lower RF in the conventional MR results from the high amount of hydrogen produced by reaction compared to the low amount separated. Looking at the other two distributions, they provide quite similar values of RY and $x$.

As regards the counter-current flow (Figure 16), the situation is similar to the co-current from a qualitative point of view, but here the performances are generally higher than before, except for the conversion in the reference distribution and for the maximized RY.

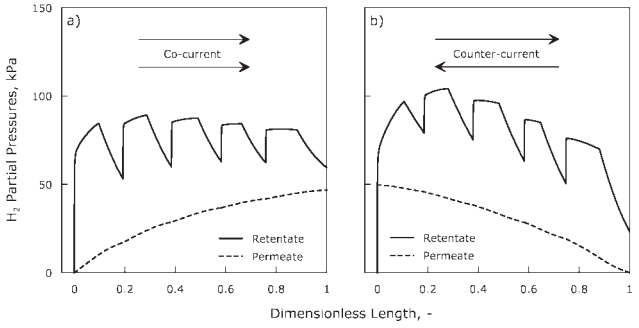


**Figure 11. $H_2$ partial pressure profiles along the reactor length on both the membrane sides for the distribution obtained from the maximization of the $H_2$ Recovery Yield in (a) co- and (b) counter-current flow.**

The arrows indicate the sense of the stream flow. The operating conditions are specified in Table 2.

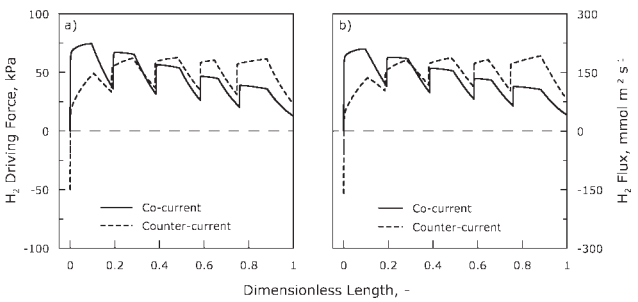


**Figure 12. (a) Hydrogen permeation driving force and (b) transmembrane flux profiles along the reactor length for the catalyst distribution obtained from the maximization of the $H_2$ Recovery Yield in co- and counter-current flow.**

The operating conditions are specified in Table 2.

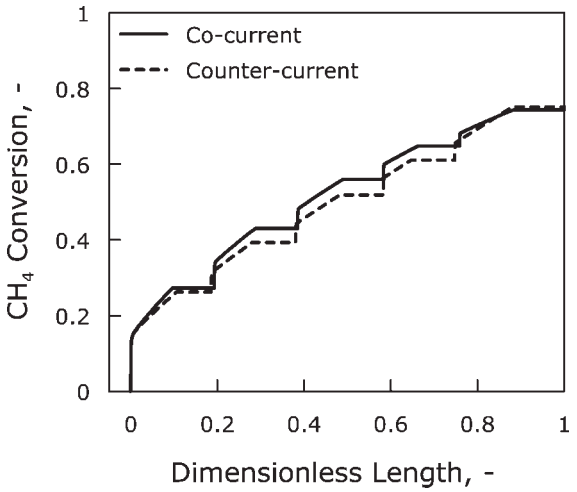


**Figure 13. Conversion profiles for the catalyst distribution obtained from the maximization of the $H_2$ Recovery Yield in co- and counter-current flow.**

The operating conditions are specified in Table 2.

Furthermore, in this second case, the differences between the various distributions are slightly larger than those in the previous situation. In fact, RF in the reference configuration is higher than that in MR of about 11%, against the previous value of 3.5%. A very interesting point is that RY of the MR in co-current (Figure 15) is the same as the one of the SMR obtained in condition of maximum RY in counter-current (Figure 16). This means that, only by changing the configuration flow, it is possible to achieve the same performance (at least in terms of RY) as the conventional MR with one half of the catalyst mass. This does not occur considering the conversion, since it is natural that, in conditions far enough from equilibrium, a larger amount of catalyst provides a higher conversion.

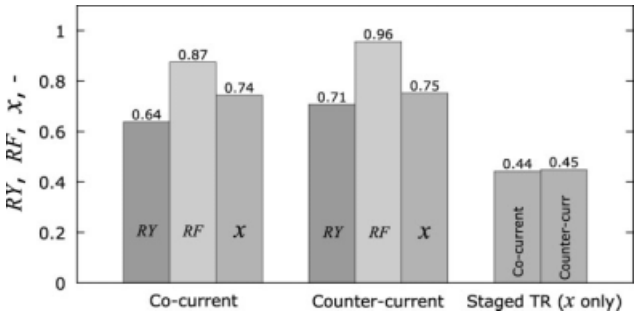


**Figure 14. Reactor performances in terms of recovery yield RY, recovery factor RF and conversion *x* in co- and counter-current flow for the catalyst distribution obtained from the maximization of the $H_2$ Recovery Yield.**

The conversion of the corresponding staged TR is also reported for comparison in both the flow configurations. The operating conditions are specified in Table 2.

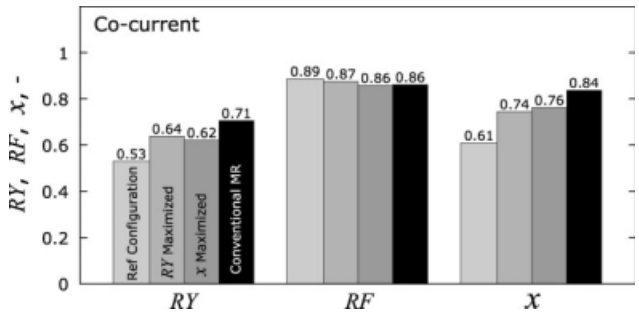


**Figure 15. Comparison among the SMR performances for several catalyst distributions in co-current flow.**

The performances of the conventional MR (with the same membrane area as the SMR but a double amount of catalyst) are also reported. The operating conditions are specified in Table 2.

## Conclusions

In the present work a computational model of a membrane reactor is used to analyse the steam reforming of methane under staged operation. The reactor consists of reactive/permeative stages in series to inert/permeative stages of variable lengths. The optimal distribution of stage lengths is found by maximizing performance indices such as the methane conversion, the hydrogen RF and RY. The system is studied considering co- and counter-current flow conditions. The results show that the counter-current flow provides always significantly better performances than the co-current one. As concerns the shape of the distribution obtained, the analysis reveals that an almost equi-sized distribution is achieved by maximizing the RF in both the configuration flow, whereas, when maximizing the conversion, the optimization procedure provided a negligible last inert stage. The fact that the performances of the ten-staged MRs are significantly higher than the ones of the reference membrane reactor (two-staged one) in terms of conversion and RY suggests that the

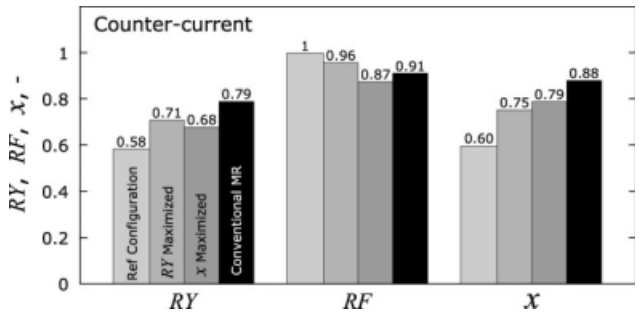


**Figure 16. Comparison among the SMR performances for several catalyst distributions in counter-current flow. The performances of the conventional MR (with the same membrane area as the SMR but a double amount of catalyst) are also reported.**

The operating conditions are specified in Table 2.

number of stages represents a very important variable for leading to a more profitable use of catalyst and, in general, raw materials. This topic will be studied in the part II of the present article.[22]

## Acknowledgments

A. Caravella is grateful to the "Repubblica Italiana, Ministero dell'Università e della Ricerca (MiUR)" for the financial support in the frame of the Center of Excellence CEMIF.CAL (CLAB01TYEF). This work is part of the FIRB-CAMERE (RBNE03JCR5) project, funded by the "Ministero dell'Università e della Ricerca (MiUR)" that is gratefully acknowledged.

## Notation

$A$ = cross-sectional area ($m^2$)
$D_m$ = membrane mean diameter (m)
$D_{Eq}$ = equivalent diameter (m)
$d_p$ = mean pellet diameter (m)
$E_d$ = permeance activation energy (J/mol)
$F$ = molar flow rate (mol/s)
$h$ = heat transfer coefficient [J/(s $m^2$ K)]
$\Delta H$ = molar enthalpy (J/mol)
$\Delta H_r^0$ = reaction molar enthalpy at the standard state (J/mol)
ID, OD = inner, outer diameter (m)
$k$ = thermal conductivity [J/(s m K)]
$l$ = stage length (m)
$m^{Ret}$, $m^{Perm}$ = number of species in the retentate and permeate side (−)
$n^R$, $n^I$ = number of reactive ($n^R$) and inert ($n^I$) stages (−)
$n^{Stages}$ = total number of stages (−)
$N_i$ = molar permeating flux [mol/($m^2$ s)]
$P$ = total pressure (Pa)
$P_i$ = partial pressure (Pa)
$Pr$ = Prandtl Number (−)
$R$ = ideal gas constant [J/(mol K)]
$Re$ = Reynolds number (−)
$Re_p$ = Reynolds number for packed beds (−)
$R_i$ = rate of formation of the $i$th species [mol/(s $m^3$)]
$T$ = temperature (K)
$U$ = overall heat transfer coefficient [J/(s $m^2$ K)]
$v$ = velocity (m/s)
$y_{catalyst}$ = amount of catalyst (%)
$x$ = methane conversion (−)
$z$ = abscissa (m)

### *Greek letters*

$\alpha$ = exponent in the $H_2$ permeation law (−)
$\delta$ = thickness (m)
$\varepsilon$ = voidage (−)
$\kappa$ = permeability pre-exponential factor [mol/(m s $Pa^n$)]
$\eta$ = effectiveness factor (−)

### *Subscripts*

Mix = mixture
Supp = membrane support

### *Superscripts*

Cat = catalytic bed
Ext = external
Fur = furnace
Mem = membrane
Min = minimum
SS = stainless steel
Tot = total (referred to the reactor length)
TM = trans-membrane

### *Acronyms*

MR = conventional membrane reactor
SMR = staged membrane reactor
RF = $H_2$ recovery factor (−)
RY = $H_2$ recovery yield (−)
TR = traditional reactor

## Literature Cited

1. Dittmeyer R, Höllein V, Daub K. Membrane reactors for hydrogenation and dehydrogenation processes based on supported palladium. *J Mol Catal A: Chem*. 2001;173:135–184.
2. Keil JK. *Modeling of Process Intensification*. Weinheim: Wiley-VCH Verlag GmbH KGaA, 2007.
3. Tong J, Matsumura Y. Thin Pd membrane prepared on macroporous stainless steel tube filter by an in-situ multidimensional plating mechanism. *Chem Commun*. 2004;2460–2461.
4. Tong J, Su L, Haraya K, Suda H. Thin and defect-free Pd-based composite membrane without any interlayer and substrate penetration by a combined organic and inorganic process. *Chem Commun*. 2006;1142–1144.
5. Ciocco MV, Morreale BD, Rothenberger KS, Howard BH, Cugini AV, Killmeyer RP, Enick RM. High-pressure, high-temperature hydrogen permeability measurements of supported thin-film palladium membranes. In: Proceedings of the Pittsburgh Coal Conference, Pittsburgh PA, 2003.
6. Pan X, Kilgus M, Goldbach A. Low-temperature $H_2$ and $N_2$ transport through thin $Pd_{66}Cu_{34}H_x$ layers. *Catal Today*. 2005;104:225–230.
7. Gielens FC, Tong HD, Vorstman MAG, Keurentjes JTF. Measurement and modeling of hydrogen transport through high-flux Pd membranes. *J Memb Sci*. 2007;289:15–25.
8. Guazzone F, Engwall EE, Ma YH. Effects of surface activity, defects and mass transfer on hydrogen permeance. *Catal Today*. 2006;118:24–31.
9. Barbieri G, Scura F, Lentini F, De Luca G, Drioli E. A novel model equation for the permeation of hydrogen in mixture with carbon monoxide through Pd-Ag membranes. *Separat Purif Technol*. 2008;61:217–224.
10. Koukou M, Papayannakos N, Markatos N. On the importance of non-ideal flow effects in the operation of industrial-scale adiabatic membrane reactors. *Chem Eng J*. 2001;83:95–105.
11. Assabumrungrat S, Suksomboom K, Praserthdam P, Tagawa T, Goto S. Simulation of palladium membrane reactor for dehydrogenation of ethylbenzene. *J Chem Eng Jpn*. 2002;35:263–273.
12. Marigliano G, Barbieri G, Drioli E. Effect of energy transport on a palladium-based membrane reactor for methane steam reforming process. *Catal Today*. 2001;67:85–99.
13. Lin Y, Liu S, Chuang C, Chu Y. Effect of incipient removal of hydrogen through palladium membrane on the conversion of methane steam reforming: experimental and modeling. *Catal Today*. 2003;82:127–139.
14. Oklany J, Hou K, Hughes R. A simulative comparison of dense and microporous membrane reactors for the steam reforming of methane. *Appl Catal A: Gen*. 1998;170:13–22.
15. Adris AM, Lim CJ, Grace JR. The fluidized-bed membrane reactor for steam methane reforming: model verification and parametric study. *Chem Eng Sci*. 1997;52:1609–1622.
16. Chiappetta G, Clarizia G, Drioli E. Theoretical analysis of the effect of catalyst mass distribution and operation parameters on the performance of a Pd-based membrane reactor for water-gas shift reaction. *Chem Eng J*. 2008;136:373–382.
17. Caravella A, Di Maio FP, Di Renzo A. Optimization of membrane area and catalyst distribution in a permeative-stage membrane reactor for methane steam reforming. *J Memb Sci*. 2008;321:209–221.
18. Li A, Lim CJ, Grace JR. Staged-separation membrane reactor for steam methane reforming. *Chem Eng J*. 2008;138:452–459.
19. Quang DV, Ham P, Gelas D, Legrand C. Apparatus for performing chemical reactions under pressure in a multi-stage reaction zone with external intermediary thermal conditioning, US Patent 0,051,925, 112A, 1993.
20. Vanderborgh N. Device for staged addition of heat to a reactor, US Patent 2002/0,098,136 A1, 2002.
21. Hemmings JW, Bonnell L, Robinson ET. Synthesis gas production method and reactor, US Patent 0,292,342 A1, 2007.

22. Caravella A, Di Maio FP, Di Renzo A. Computational study of staged membrane reactor configuration for methane steam reforming: II. Effect of number of stages and catalyst amount. *AIChE J*. 2010;56(1):259–267.
23. Tong J, Matsumura Y, Suda H, Haraya K. Experimental study of steam reforming of methane in a thin (6 $\mu$m) Pd-based membrane reactor. *Ind Eng Chem Res*. 2005;44:1454–1465.
24. Xu J, Froment GF. Methane steam reforming, methanation and water-gas shift: I. Intrinsic kinetics. *AIChE J*. 1989;35:88–96.
25. Harriot P. *Chemical Reactor Design*. New York: Marcel Dekker, *Chapter 6*, 2003:249–255.
26. Ward T, Dao T. Model of hydrogen permeation behavior in palladium membranes. *J Memb Sci*. 1999;153:211–231.
27. Caravella A, Barbieri G, Drioli E. Modelling and simulation of hydrogen permeation through supported Pd-based membranes with a multicomponent approach. *Chem Eng Sci*. 2008;63:2149–2160.
28. Sodrè JR, Parise JAR. Fluid flow pressure drop through an annular bed of spheres with wall effects. *Exp Therm Fluid Sci*. 1998;17:265–275.
29. The MathWorks Inc. MATLAB [Online], available at http://www.mathworks.com/products/matlab/.
30. Froment GF. *Chemical Reactor Analysis and Design*. New York: Wiley, 1990.
31. Kern DQ. *Process Heat Transfer*. Chap. *6*, New York: McGraw-Hill, 1997:103–104.

## Appendix A

### *Evaluation of the Heat Transfer Coefficient*

The expressions for the calculation of the furnace-shell ($U^{Ext}$) and shell-tube ($U^{TM}$) heat transfer coefficients are based on a series of resistances, as illustrated in the sketch reported in Figure A1. The temperature of the external wall is assumed equal to that of the furnace.

The external and transmembrane overall heat transfer coefficients are expressed as reported in Eq. A1. where the outer areas are used as a reference for the shell and tube side.

$$\frac{1}{U^{Ext}} = \frac{OD^{Shell}}{2k_{SS}} ln\left(\frac{OD^{Shell}}{ID^{Shell}}\right) + \frac{OD^{Shell}}{ID^{Shell}} \frac{1}{h^{Shell}} \quad (A1)$$

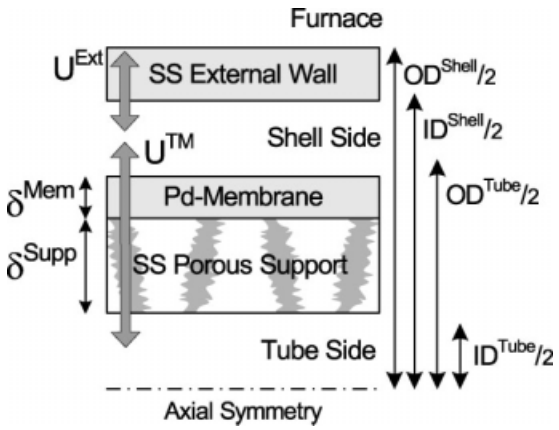


**Figure A1. Scheme of the porous stainless steel supported Pd-alloy membrane considered in this analysis.**

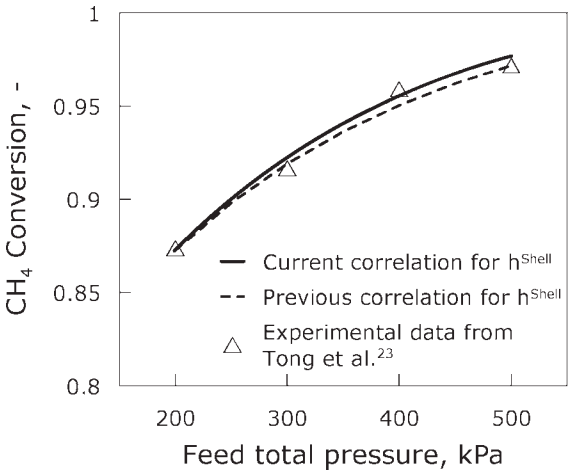


**Figure A2. Comparison among experimental data of Tong et al.,[23] previous correlation for the calculation of the heat transfer coefficient and current correlation used in this work.**

$$\frac{1}{U^{TM}} = \frac{1}{h^{Shell}} + \frac{OD^{Tube}}{2k^{Mem}} ln\left(\frac{OD^{Tube}}{ID^{Tube} + 2\delta^{Supp}}\right) + \frac{OD^{Tube}}{2k^{Supp}} ln\left(\frac{ID^{Tube} + 2\delta^{Supp}}{ID^{Tube}}\right) + \frac{OD^{Tube}}{ID^{Tube}} \frac{1}{h^{Tube}} \quad (A2)$$

The thermal conductivity of the porous support $k^{Supp}$ is shown in Eq. A3., where $k_{SS}$ and $k_{Mix}^{Perm}$ are the thermal conductivities of the stainless steel and of the gaseous mixture in the tube (permeate) side, respectively.

$$k^{Supp} = (1 - \varepsilon_{Supp})k_{SS} + \varepsilon_{Supp}k_{Mix}^{Perm} \quad (A3)$$

where the packed bed is present, the heat transfer coefficient between the fluid and walls is evaluated from Eq. A4,[30] otherwise, the correlation shown in Eq. A5[31] is used.

$$h^{Shell} = 0.813 \frac{k_{Mix}^{Ret}}{D_{Eq}^{Shell}} \exp\left(-\frac{6d_p}{D_{Eq}^{Shell}}\right) Re_p^{0.9}, \quad Re_p = \frac{\rho v d_p}{\mu} \quad (A4)$$

$$h = 0.027 \frac{k_{Mix}}{D_{eq}} Re^{0.8} Pr^{\frac{1}{3}} \quad (A5)$$

The correlation for the calculation of the heat transfer coefficient used in the present article (Eq. A4) has been compared to the same experimental validation provided in a previous article[17] showing in fact the same behavior, as demonstrated in Figure A2.

*Manuscript received Dec. 10, 2008, and revision received Apr. 6, 2009.*